Journal of Thermal Analysis and Calorimetry, Vol. 83 (2006) 1, 97–106

USING A QUASI-HEAT-PULSE METHOD TO DETERMINE HEAT AND MOISTURE TRANSFER PROPERTIES FOR POROUS ORTHOTROPIC WOOD PRODUCTS OR CELLULAR SOLID MATERIALS*

*M. A. Dietenberger***

USDA Forest Service, Forest Products Laboratory, One Gifford Pinchot Drive, Madison Wisconsin 53726-2398

Understanding heat and moisture transfer in a wood specimen as used in the K-tester has led to an unconventional numerical solution and intriguing protocol to deriving the transfer properties. Laplace transform solutions of Luikov's differential equations are derived for one-dimensional heat and moisture transfer in porous hygroscopic orthotropic materials and for a gradual finite heat pulse applied to both surfaces of a flat slab. The K-tester 637 (Lasercomp) supplies a quasi-heat-pulse to both sides of a 2-ft-square specimen and records precise signals as function of time from surface thermocouples and heat flux thermopiles. We obtained transfer properties for moist and oven-dried redwood lumber flooring.

Keywords: *cellular solid materials, heat/moisture transfer properties, Luikov equations solutions, porous orthotropic wood*

Introduction

With wood being orthotropic, a practical test method must be limited to high-aspect-ratio flat slab geometry, which eliminates many short-pulse heat methods provided in the literature [1–3]. Methods using sustained heat pulse or steady-state conditions [4, 5] are subject to strong moisture migration effects, which can lead to confusion or inconsistencies in the derived heat and moisture transfer properties. Difficulties in measuring moisture and temperature profiles within a solid wood specimen, for deriving moisture- and temperature-dependent properties, preclude methods developed for soft organic matter. In this method we derived an analytical Laplace transform solution to the Luikov's differential equations for one-dimensional heat and moisture transfer [6–9] and for a gradual finite heat pulse applied to both surfaces of a flat slab. The result is a rapid moisture wave being thermally driven into the slab and then a gradual settling back to the original uniform moisture upon heat pulse removal. This moisture movement also involves the latent heat of water, which significantly perturbs the conductive heat transfer process. Note that this quasi-heat-pulse method preserves the average moisture content of the wood slab and prevents severe gradients from occurring along the slab so as to preserve one-dimensional flow processes across the slab. The moist, porous, temperature-dependent, and orthotropic wood under constant pressure has the coupled transient heat and mass transfer equations [6] as

$$\rho C_q \frac{\partial T}{\partial t} = \nabla\cdot(K_q\cdot\nabla T) + \varepsilon\lambda\rho C_m \frac{\partial U}{\partial t} + g_q(\vec{r},t) \quad (1)$$

$$\rho C_m \frac{\partial U}{\partial t} = \nabla\cdot(K_m\cdot[\nabla U+\delta\nabla T]) + g_m(\vec{r},t) \quad (2)$$

where T is temperature, U moisture potential, t time, K_q and K_m are thermal and moisture conductivity coefficients, C_q and C_m are heat and moisture capacities, $g_q(\vec{r},t)$ and $g_m(\vec{r},t)$ are heat and mass generations as direct functions of position and time, respectively, ρ is dry body density, ε ratio of vapor diffusion coefficient to coefficient of total moisture diffusion, λ heat of phase change, and δ the thermogradient coefficient. The simplest situation is to apply a steady heat flux, but zero mass flux, across the boundaries in a principal direction of the material. This zeroes the term $\nabla U + \delta\nabla T$ in that principal direction and thus defines the moisture migration condition at steady state. Consequently one obtains a constant heat flux $\vec{q}^{\ell} = K_q\cdot\nabla T$ across the principal direction. The thermal conductivity K_q and mass conductivity K_m are considered matrix variables for representing anisotropic material, and the off-diagonal terms are zero for principal directions or for orthotropic materials [10]. However, the use of a steady-state apparatus for high-aspect-ratio samples is not as simple, because the thermal conductivity and mass conductivity [6] generally in-

* This paper was prepared by U.S. Government employees on official time and is therefore in the public domain and not subject to copyright in the United States

** mdietenberger@fs.fed.us

1388–6150/$20.00

Akadémiai Kiadó, Budapest, Hungary
Springer, Dordrecht, The Netherlands

crease with both temperature T and moisture content $C = C_m U$. The result is a non-linear distribution of both temperature and moisture content across the sample thickness. Likewise, another simple situation is to apply a constant mass flux, but zero heat flux, across the boundaries in a principal direction of the material. By measuring both temperature and moisture profiles within the sample in this test procedure, the value of mass conductivity K_m can also be derived as function of temperature and moisture content. The heat capacity C_q and heat of phase change λ are assumed available from differential scanning calorimeter measurements or another method. This two-step procedure was used for evaluating certain food materials, such as bread [11]. However, the procedure is implemented rarely for wood materials because of the difficulty of obtaining reliable simultaneous temperature and moisture profiles within the sample.

As an alternative, one can take advantage of the mass diffusivity as being two orders of magnitudes less than thermal diffusivity. This approach utilizes specialized transient methods [6]; that is, to obtain moisture conductivity K_m, the sample should be subjected to a sustained change in moisture loss rate while keeping its temperature at a steady value, as approximately in a high-velocity, very dry convective environment. On the other hand, for obtaining the thermal properties C_q and $K_{eff} = K_q + \varepsilon\lambda\delta K_m$, a short heat conductive pulse should be applied to the sample in a way that allows the thermal wave to dissipate fairly rapidly. While the sample gradually reaches some uniform temperature, any slight perturbation in the moisture profile due to heat-pulse-generated water flux $\vec{m}_q'' = \delta K_m \cdot \nabla T$ is gradually flattened back to the original uniform moisture profile by moisture gradients. Thus, we have Eq. (1) during the early transient regime, which can be approximated as

$$\rho C_q \frac{\partial T}{\partial t} \cong \nabla \cdot (K_{eff} \cdot \nabla T) \tag{3}$$

This experimental design in using heat-pulse profile would then cause only a small perturbation in the uniform moisture profile, thereby allowing us to ignore Eq. (2) and the moisture gradient term in Eq. (1). Analytical (and CFD) solutions of Eq. (3) subject to various boundary conditions can be found in standard heat conduction texts [10]. If the perturbing moisture profile is too great, then the coupled Eqs (1) and (2) need to be solved, for which only a few analytical solutions are available. One also realizes the steady-state value for thermal conductivity, K_q, is generally less than the transient value for thermal conductivity, K_{eff}, a situation often overlooked by some researchers but not validated. Indeed, this factor could cause confusion in related fields, such as calculating time to ignition for wood exposed to high irradiance using derived thermal properties. Here we provide such validation by providing a general quasi-analytical solution to Eqs (1) and (2).

The overall heat–mass transfer solution is formulated in four phases: The first phase is to transform coupled Eqs (1) and (2) into an analytically solvable form by imposing constant, unidirectional surface boundary conditions on both faces of a finitely thick high-aspect-ratio slab and assuming that temperature- and moisture-dependent properties are constant during the exposure. The second phase involves application of the Duhamel's integral theorem for non-linear boundary conditions. Modern computer data acquisition makes this method feasible through measuring heat and mass losses in small time steps, thus making the theoretical solution quasi-analytical. In the third phase, we allow variations in temperature and moisture dependency in properties (capacities and conductivities now are specific functions of temperature and moisture content) with the analytical solution by additional transformations of the variables. The fourth phase involves analytical transient solutions for the walls of the specimen box and K-tester to provide 'corrected' boundary conditions. This quasi-analytical solution is amenable to non-linear least squares regression routines used in spreadsheets. This promising technique is now formalized.

Solution with constant properties and boundary conditions

For time-invariant properties and sources and with unidirectional boundary conditions, Eqs (1) and (2) are transformed to a symmetric Laplace transform as

$$s\overline{T}(x,s) - T_o(x) = \alpha^* \frac{\partial^2 \overline{T}(x,s)}{\partial x^2} + \alpha^* \delta^* \frac{\partial^2 \overline{U}(x,s)}{\partial x^2} + \frac{g_q(x)}{s} \tag{4}$$

$$s\overline{U}(x,s) - U_o(x) = \alpha_m \frac{\partial^2 \overline{U}(x,s)}{\partial x^2} + \alpha_m \delta \frac{\partial^2 \overline{T}(x,s)}{\partial x^2} + \frac{g_m(x)}{s} \tag{5}$$

where

$$\alpha^* = \frac{K_q + \varepsilon\lambda K_m \delta}{\rho C_q} = \alpha_q + \frac{\varepsilon\lambda K_m \delta}{\rho C_q} \tag{6}$$

$$\delta^* = \frac{\varepsilon\lambda K_m}{K_q + \varepsilon\lambda K_m \delta} \tag{7}$$

$$\alpha_m = \frac{K_m}{\rho C_m} \tag{8}$$

Likewise, time-invariant boundary conditions during a process have similar symmetric transformations. Because we will convert Eqs (4) and (5) to a system of four first-order linear differential equations and solve using a rigorous matrix algebra technique [12], the appropriate and easiest boundary conditions are those prescribed completely on one surface (at the origin) as

$$\bar{T}(0,s) = \frac{T(0,t>0)}{s} \tag{9}$$

$$\frac{\partial \bar{T}(0,s)}{\partial x} + \delta^* \frac{\partial \bar{U}(0,s)}{\partial x} = \frac{\dot{q}''_{\ell}(0,t>0)}{(K_q + \varepsilon\lambda K_m \delta)s} \tag{10}$$

$$\bar{U}(0,s) = \frac{U(0,t>0)}{s} \tag{11}$$

$$\frac{\partial \bar{U}(0,s)}{\partial x} + \delta \frac{\partial \bar{T}(0,s)}{\partial x} = \frac{\dot{m}''_{\ell}(0,t>0)}{(K_m)s} \tag{12}$$

At initial time, temperature and moisture are at initial values, $T_0(x)$ and $U_0(x)$, respectively. The solution to Eqs (4) and (5) as subject to the boundary conditions, Eqs (9) to (12), can be used to solve for values and gradients of temperature and moisture at the material's thickness; that is, there are essentially eight choices for boundary conditions (four for each surface), of which only four are needed to obtain a unique solution. Thus, 8!/4!4! = 70 distinct solutions are possible, but in this short paper we provide just a few examples and omit the mathematical process descriptions. We note, however, that the homogeneous solutions to Eqs (4) and (5), after a detailed algebraic manipulation, have simple hyperbolic sine and cosine functions along with simple expressions for the eigenvalues of the matrix equation. This should allow us to examine a variety of analytical functions for the non-homogeneous terms and analytically solve for the general solution of combined temperature and moisture profile as function of time. For example, if wood has a sudden change in thermal–moisture properties, as in a dry-out or degradation, then we use the 'restart' profiles, $T_0(x) = T(x,t_d)$ and $U_0(x) = U(x,t_d)$, so that the temperature–moisture solution can then proceed after time of degradation using the degraded properties. In another example, microwave heating with wood depth can be represented by the heat generation term $g_q(x)$, and wood-structure dehydration during heated degradation can be represented by moisture generation term $g_m(x)$. These non-homogeneous factors are beyond the scope of this paper. However, eliminating these non-homogeneous processes requires careful experimental test design that begins with low uniform temperature and moisture profiles and then allowing only a small jump in temperature or moisture content for a test run.

Table 1 The three-step solution with boundary conditions for the components in K-tester 637

Components	First step	Second step	Third step
Upper thermopile with FR4 layer and water heat pulsing	T_{UW} = data; U_{UW} = 0 XXXXXXXXXX T_{UF} = data ; U_{UF} = 0		
Upper copper cladding layer of thermopile		$T_{UC} = T_{UF}$; $\dot{q}''_{UC} = \dot{q}''_{UF}$ U_{UC} = 0; $\dot{m}''_{UC}$ = 0 XXXXXXXXXXXX	
Upper 0.4-mm-thick aluminum plate		$T_{UA} = T_{UC}$; $\dot{q}''_{\ell UA} = \dot{q}''_{UC}$ U_{UA} = 0; $\dot{m}''_{UA}$ = 0 XXXXXXXXXXXX	
25.4-mm-thick XPS foam or wood test specimen	[Solve for T and $\dot{q}''$ in thermopiles from Eq. (18)]	[Solve for T and $\dot{q}''$ in thin aluminum plates (and copper claddings) from Eq. (16)]	$\dot{q}''_{\ell US} = \dot{q}''_{UA}$; $\dot{m}''_{US}$ = 0 XXXXXXXXXXXX [Solve for T, T', U, and U' from Eq. (20)] XXXXXXXXXXXX $\dot{q}''_{\ell LS} = \dot{q}''_{\ell LA}$; $\dot{m}''_{LS}$=0
Lower 0.4-mm-thick aluminum plate		XXXXXXXXXXXX $T_{LA} = T_{LC}$; $\dot{q}''_{LA} = \dot{q}''_{LC}$ U_{LA}=0; $\dot{m}''_{LA}$= 0	
Lower copper cladding layer of thermopile		XXXXXXXXXXXX $T_{LC} = T_{LF}$; $\dot{q}''_{LC} = \dot{q}''_{LF}$ U_{LC} = 0; $\dot{m}''_{LC}$ = 0	
Lower thermopile with FR4 layer and water heat pulsing	T_{LF} = data ; U_{LF} = 0 XXXXXXXXXX T_{LW} = data; U_{LW} = 0		

T = temperature, U = moisture potential, U = upper layers, L = lower layers, W = water side, F = thermopile, C = copper cladding, A = Aluminum plate, S = specimen, $\dot{q}''_{\ell}$ = heat flux, and $\dot{m}''_{\ell}$ = water mass flux, XXXXXXXX = Material layer representation

Homogeneous solutions of three relevant boundary conditions

In solving the transient heat and mass transfer problem for the K-tester, it is required to proceed in a three-step process, as shown schematically in Table 1. When the K-tester applies a heat pulse across the upper and lower FR4 layers, the responses in these layers are recorded with the thermocouple and thermopile data. Therefore, temperatures as functions of time are known at the surfaces of the FR4 material, for which in applying a transient heat transfer solution we derived the transient heat flux at the surface of the copper cladding. This in turn allows us to solve for transient heat transfers in the copper cladding and aluminum plate covering the specimen. These solutions provide the actual time-delayed heat fluxes that will be experienced by both surfaces of the test specimen. The use of the aluminum plates also ensures that the surface water fluxes are equal to zero. The corresponding solution for heat and moisture transfer in the specimen provide the profile for temperature and moisture content values, which then are compared to the actual surface temperature values at the interfaces of aluminum plate and the test specimen. To obtain close agreement in their temperature values over the entire test time period, the values for the thermophysical properties of the specimen are adjusted iteratively. We note that the K-tester has the specimen surrounded by highly reflective, insulating, conformable and sealed interior walls and has a 10- by 10-cm center sensing area that we use for the unidirectional heat flow data.

The corresponding impact on solving Eqs (1) and (2) from a mathematical viewpoint is to consider only three relevant boundary conditions (BCs), although 70 usable boundary conditions are possible. The first is specifying surface values and gradients of temperature–moisture on just one side of a material. The aluminum skin covering over some samples and copper surface cladding in the K-tester will be represented by this solution, although we would simplify it by striking out the moisture terms. The second BC is specifying just the surface values of temperature–moisture on both sides of a material. The K-tester's thermopile will be represented by this solution, although we will also simplify it by striking out the moisture terms. The third BC–the most important–is the specification of just the surface gradients on both surfaces of a material. The wood product to be tested will be represented by this solution. Indeed, by heating the specimen equally on both sides in the K-tester apparatus, no moisture mass flow would occur on specimen surfaces at any time.

The first boundary condition is Eqs (9) to (12) and is coupled with the generic homogeneous solutions of Eqs (4) and (5). Taking inverse Laplace transforms of the resulting equations and applying the Duhamel's integral theorem for non-linear boundary conditions [10], we obtain the following time domain solution. First we make use of the convenient functions

$$P(a,\hat{x},t)=L^{-1}\left(\frac{\cosh(\hat{x}\ell\sqrt{as})}{s}\right) =1-\frac{4}{\pi}\sum_{n=0}^{\infty}\frac{1}{2n+1}\exp\left(\frac{-t}{a}\left[\frac{(2n+1)\pi}{2\ell\ell}\right]^2\right)\sin\left(\frac{(2n+1)\pi\hat{x}}{2\ell}\right) \quad (13)$$

$$Q(a,\hat{x},t)=L^{-1}\left(\frac{\sinh(\hat{x}\ell\sqrt{as})}{s\sqrt{as}}\right)=\hat{x}\ell\otimes\frac{8\ell\ell}{\pi^2}\sum_{n=0}^{\infty}\frac{1}{(2n+1)^2}\exp\left(\frac{-t}{a}\left[\frac{(2n+1)\pi}{2\ell}\right]^2\right)\left(1-\cos\left[\frac{(2n+1)\pi}{2\ell}\right]\right) \quad (14)$$

$$a=\frac{\alpha_m+\alpha^*}{2\alpha_m\alpha_q}+\sqrt{\left(\frac{\alpha_m+\alpha^*}{2\alpha_m\alpha_q}\right)^2-\frac{1}{\alpha_m\alpha_q}}$$
$$b=\frac{\alpha_m+\alpha^*}{2\alpha_m\alpha_q}-\sqrt{\left(\frac{\alpha_m+\alpha^*}{2\alpha_m\alpha_q}\right)^2-\frac{1}{\alpha_m\alpha_q}} \quad (15)$$

In Eqs (13) and (14) the term b replaces the term a when appropriate. The first BC solution for $T(x,t)$ and $U(x,t)$ is shown on the next page as Eq. (16).

The symbol $\otimes$ represents the convolution operation with respect to time as prescribed in the Duhamel's integral theorem. Note the expected symmetry between temperature and moisture solutions in Eq. (16). If surface moisture flow flux $\dot{m}''(0,t)$ and moisture 'capacity' C_m are set to zero, then Eq. (16) reduces to the classical heat conduction solution [10]. Indeed, the solution retains its complexity even if just surface moisture flow is zero, implying transient movement of moisture within the material that perturbs the heat conduction process.

The second boundary condition is obtained from setting $\hat{x}=\ell$ in previous equations in their transformed frequency domain and solving for gradients of surface temperature and moisture at the origin as functions of temperature and moisture values on both surfaces. Obtaining the inverse Laplace transform and applying the Duhamel's integral theorem to non-linear boundary conditions [10], the resulting time domain solution is the following. First we make use of a convenient function $R(a,x,t)$ as Eq. (17) on the next page.

$$
\begin{aligned}
T(\hat{x},t) &= T(0,t)\otimes\left(\frac{ab\alpha_m - b}{a-b}\dot{P}(a,\hat{x},t)+\frac{a-ab\alpha_m}{a-b}\dot{P}(b,\hat{x},t)\right)\\
&+\left(\frac{\dot{q}''(0,t)}{(1-\delta\delta^*)(K_q+\varepsilon\lambda K_m\delta)}-\frac{\delta^*\dot{m}''(0,t)}{(1-\delta\delta^*)(K_m)}\right)\otimes\left(\frac{ab\alpha_m - b}{a-b}\dot{Q}(a,\hat{x},t)+\frac{a-ab\alpha_m}{a-b}\dot{Q}(b,\hat{x},t)\right)\\
&+U(0,t)\otimes\left(\frac{\delta^* ab\alpha^*}{a-b}(-\dot{P}(a,\hat{x},t)+\dot{P}(b,\hat{x},t))\right)\\
&+\left(\frac{\dot{m}''(0,t)}{(1-\delta\delta^*)(K_m)}-\frac{\delta\dot{q}''(0,t)}{(1-\delta\delta^*)(K_q+\varepsilon\lambda K_m\delta)}\right)\otimes\left(\frac{\delta^* ab\alpha^*}{a-b}(-\dot{Q}(a,\hat{x},t)+Q(b,\hat{x},t))\right)\\
U(\hat{x},t) &= T(0,t)\otimes\left(\frac{\delta ab\alpha_m}{a-b}(-\dot{P}(b,\hat{x},t)+\dot{P}(b,\hat{x},t))\right)\\
&+\left(\frac{\dot{q}''(0,t)}{(1-\delta\delta^*)(K_q+\varepsilon\lambda K_m\delta)}-\frac{\delta^*\dot{m}''(0,t)}{(1-\delta\delta^*)(K_m)}\right)\otimes\left(\frac{\delta ab\alpha_m}{a-b}(-\dot{Q}(a,\hat{x},t)+\dot{Q}(b,\hat{x},t))\right)\\
&+U(0,t)\otimes\left(\frac{ab\alpha^*-b}{a-b}\dot{P}(a,\hat{x},t)+\frac{a-ab\alpha^*}{a-b}\dot{P}(b,\hat{x},t)\right)\\
&+\left(\frac{\dot{m}''(0,t)}{(1-\delta\delta^*)(K_m)}-\frac{\delta\dot{q}''(0,t)}{(1-\delta\delta^*)(K_q+\varepsilon\lambda K_m\delta}\right)\otimes\left(\frac{ab\alpha^*-b}{a-b}\dot{Q}(a,\hat{x},t)+\frac{a-ab\alpha^*}{a-b}\dot{Q}(b,\hat{x},t)\right)
\end{aligned}
\tag{16}
$$

$$
R(a,\hat{x},t)=L^{-1}\left(\frac{\sinh(\hat{x}\sqrt{as})}{s\ \sinh(\ell\sqrt{as})}\right)=\frac{\hat{x}}{\ell\ell}+\frac{2}{\pi}\sum_{n=1}^{\infty}\frac{\cos(n\pi)}{n}\exp\left[\frac{-t}{a}\left(\frac{n\pi}{\ell\ell}\right)^2\right]\sin\left(\frac{n\pi\hat{x}}{\ell\ell}\right) \tag{17}
$$

In Eq. (17) the term *b* replaces the term *a* when appropriate. The second BC solution is given by Eq. (18).

$$
\begin{aligned}
(a-b)\begin{Bmatrix}T(\hat{x},t)\\U(\hat{x},t)\end{Bmatrix} &= \begin{Bmatrix}ab\alpha_m - b\\-\delta ab\alpha_m\end{Bmatrix}[T(\ell,t)\otimes\dot{R}(a,\hat{x},t)+T(0,t)\otimes\dot{R}(a,\ell-\hat{x},t)]\\
&+\begin{Bmatrix}a-ab\alpha_m\\\delta ab\alpha_m\end{Bmatrix}[T(\ell,t)\otimes\dot{R}(b,\hat{x},t)+T(0,t)\otimes\dot{R}(b,\ell-\hat{x},t)]\\
&+\begin{Bmatrix}-\delta^* ab\alpha^*\\ab\alpha^*-b\end{Bmatrix}[U(\ell,t)\otimes\dot{R}(a,\hat{x},t)+U(0,t)\otimes\dot{R}(a,\ell-\hat{x},t)]\\
&+\begin{Bmatrix}\delta^* ab\alpha^*\\a-ab\alpha^*\end{Bmatrix}[U(\ell,t)\otimes\dot{R}(b,\hat{x},t)+U(0,t)\otimes\dot{R}(b,\ell-\hat{x},t)]
\end{aligned}
\tag{18}
$$

Indeed, this equation seems much simpler than Eq. (16). It also reduces to the classical heat conduction solution [10] if moisture capacity and change in surface moisture values are set to zero. Finally, we consider the third boundary condition, which specifies the surface fluxes of temperature and moisture, both at the origin, and the material thickness. To obtain this third boundary condition, Eq. (16) is transformed to the frequency domain s, differentiated with respect to the $\hat{x}$ variable, evaluated at $\hat{x}=\ell$, and solved for the temperature and moisture values at the origin. Obtaining the inverse Laplace transform and applying the Duhamel's integral theorem to non-linear boundary conditions [10], the resulting time domain solution is the following. First, we use the function a convenient function $S(a,x,t)$ as in following Eq. (19).

$$
\begin{aligned}
S(a,\hat{x},t) &= L^{-1}\left(\frac{\cosh(\hat{x}\sqrt{as})}{s\sqrt{as}\ \sinh(\ell\sqrt{as})}\right)=\frac{t}{a\ell\ell}+\ell\left\{\frac{3\hat{x}^2-\ell^2}{6\ell^2}-\frac{2}{\pi^2}\sum_{n=1}^{\infty}\frac{(-1)^n}{n^2}\exp\left[\frac{-t}{a}\left(\frac{n\pi}{\ell\ell}\right)^2\right]\cos\left(\frac{n\pi\hat{x}}{\ell}\right)\right\}\\
&=\sqrt{4t/a}\sum_{n=0}^{\infty}\left\{ierfc\frac{(2n+1)\ell-\hat{x}\ell}{\sqrt{4t/a}}+ierfc\frac{(2n+1)\ell+\hat{x}}{\sqrt{4t/a}}\right\}
\end{aligned}
\tag{19}
$$

In this equation the term b replaces the term a when appropriate. The third BC solution is Eq. (20).

$$
\begin{aligned}
&(1-\delta\delta^*)(a-b)\begin{Bmatrix}T(\hat{x},t)\\U(\hat{x},t)\end{Bmatrix}=\\
&\begin{Bmatrix}a-1/\alpha_{\mathrm{m}}\\-a\delta\end{Bmatrix}\left[\frac{\dot{q}''(\ell,t)}{K_{\mathrm{q},\ell\ell}+\varepsilon\lambda K_{\mathrm{m},\ell\ell}\delta}\otimes\dot{S}(a,\hat{x},t)-\frac{\dot{q}''(0,t)}{K_{\mathrm{q},0}+\varepsilon\lambda K_{\mathrm{m},0}\delta}\otimes\dot{S}(a,\ell-\hat{x},t)\right]\\
&+\begin{Bmatrix}1/\alpha_{\mathrm{m}}-b\\b\delta\end{Bmatrix}\left[\frac{\dot{q}''(\ell,t)}{K_{\mathrm{q},\ell\ell}+\varepsilon\lambda K_{\mathrm{m},\ell\ell}\delta}\otimes\dot{S}(b,\hat{x},t)-\frac{\dot{q}''(0,t)}{K_{\mathrm{q},0}+\varepsilon\lambda K_{\mathrm{m},0}\delta}\otimes\dot{S}(b,\ell-\hat{x},t)\right]\\
&+\begin{Bmatrix}-a\delta^*\\a-1/\alpha^*\end{Bmatrix}\left[\frac{\dot{m}''(\ell,t)}{K_{\mathrm{m},\ell\ell}}\otimes\dot{S}(a,\hat{x},t)-\frac{\dot{m}''(0,t)}{K_{\mathrm{m},0}}\otimes\dot{S}(a,\ell-\hat{x},t)\right]\\
&+\begin{Bmatrix}b\delta^*\\1/\alpha^*-b\end{Bmatrix}\left[\frac{\dot{m}''(\ell,t)}{K_{\mathrm{m},\ell\ell}}\otimes\dot{S}(b,\hat{x},t)-\frac{\dot{m}''(0,t)}{K_{\mathrm{m},0}}\otimes\dot{S}(b,\ell-\hat{x},t)\right]
\end{aligned}
\tag{20}
$$

Again this formula reduces to the classical heat conduction solution [10] when moisture capacity and surface water flux are set to zero. Equation (20) is particularly useful for relatively thick materials because the response function given by Eq. (19) is rapidly convergent. As an example, if we terminate with the fifth term (n = 5) in the first series of Eq. (19), we can be assured of least nine significant digits accuracy for the effective Fourier number $t/a\ell^2$ greater than 0.046. time or space has been used. The discretization of time will now be required because the convolutions resulting from the use of the Duhamel's integral theorem are very difficult to solve on an analytical basis. However, if the time steps are small enough, then the convolutions can be evaluated numerically. Indeed, by representing the boundary conditions as approximately stepping functions, the time discretization form of Eq. (20) is

$$
\begin{aligned}
&(1-\delta\delta^*)(a-b)\begin{Bmatrix}T(\hat{x},t)\\U(\hat{x},t)\end{Bmatrix}\cong\\
&\sum_{i=0}^{n}\begin{Bmatrix}a-1/\alpha_{\mathrm{m}}\\-a\delta\end{Bmatrix}\left[\frac{\Delta\dot{q}''(\ell,t_{\mathrm{i}})}{K_{\mathrm{q,l}}+\varepsilon\lambda K_{\mathrm{m},\ell\ell}\delta}S(a,\hat{x},t-t_{\mathrm{i}})-\frac{\Delta\dot{q}''(0,t_{\mathrm{i}})}{K_{\mathrm{q},0}+\varepsilon\lambda K_{\mathrm{m},0}\delta}S(a,\ell-\hat{x},t-t_{\mathrm{i}})\right]\\
&+\sum_{i=0}^{n}\begin{Bmatrix}1/\alpha_{\mathrm{m}}-b\\b\delta\end{Bmatrix}\left[\frac{\Delta\dot{q}''(\ell,t_{\mathrm{i}})}{K_{\mathrm{q},\ell\ell}+\varepsilon\lambda K_{\mathrm{m},\ell\ell}\delta}S(b,\hat{x},t-t_{\mathrm{i}})-\frac{\Delta\dot{q}''(0,t_{\mathrm{i}})}{K_{\mathrm{q},0}+\varepsilon\lambda K_{\mathrm{m},0}\delta}S(b,\ell-\hat{x},t-t_{\mathrm{i}})\right]\\
&+\sum_{i=0}^{n}\begin{Bmatrix}-a\delta^*\\a-1/\alpha^*\end{Bmatrix}\left[\frac{\Delta\dot{m}''(\ell,t_{\mathrm{i}})}{K_{\mathrm{m},\ell\ell}}S(a,\hat{x},t-t_{\mathrm{i}})-\frac{\Delta\dot{m}''(0,t_{\mathrm{i}})}{K_{\mathrm{m},0}}S(a,\ell-\hat{x},t-t_{\mathrm{i}})\right]\\
&+\sum_{i=0}^{n}\begin{Bmatrix}b\delta^*\\1/\alpha^*-b\end{Bmatrix}\left[\frac{\Delta\dot{m}''(\ell,t_{\mathrm{i}})}{K_{\mathrm{m},\ell\ell}}S(b,\hat{x},t-t_{\mathrm{i}})-\frac{\Delta\dot{m}''(0,t_{\mathrm{i}})}{K_{\mathrm{m},0}}S(b,\ell-\hat{x},t-t_{\mathrm{i}})\right]
\end{aligned}
\tag{21}
$$

Although the second series solution has somewhat more algebra, it is an even more rapidly converging series. That is, if we terminate the second series with n = 0 and n = 1, respectively, we can be assured of least nine significant digits accuracy for the effective Fourier numbers less than 0.06 and 0.1, respectively. We utilize these computational results as follows.

Implementation for use in a spreadsheet

Up to this point, the solution for heat and moisture transfer has been analytical, as no discretization of

Equations (16) and (18) are similarly time discretized. Intuitively, this time discretization solution is just a series of innumerous micro-thermal/mass-waves into the material. One downfall of this approach is that the computational effort then increases parabolically in the form given above, making it impractical for many cases. However, close examination of the response function in Eq. (19) suggests conversion to a fully recursive form shown by Eqs (22) and (23).

The accumulating recursive terms $I_{\mathrm{f,m}}$ and $J_{\mathrm{f,n,m}}$ are substituted for the appropriate terms in descretized form of Eqs (16), (18), and (20) (and using

$$I_{\mathrm{f,m}} \equiv \sum_{\mathrm{i}=0}^{\mathrm{m}} \Delta f(t_{\mathrm{i}}) \left(\frac{t_{\mathrm{m}+1} - t_{\mathrm{i}}}{a\ell\ell} + \ell\ell \frac{3\hat{x}^2 - \ell\ell}{6\ell\ell} \right)$$
$$= I_{\mathrm{f,m}-1} + (f(t_{\mathrm{m}+1/2}) - f(t_{0-1/2})) \left(\frac{t_{\mathrm{m}+1} - t_{\mathrm{m}}}{a\ell\ell} \right) + \Delta f(t_{\mathrm{m}}) \left(\ell\ell \frac{3\hat{x}^2 - \ell^2}{6\ell\ell} \right) \tag{22}$$

$$J_{\mathrm{f,n,m}} = \sum_{\mathrm{i}=0}^{\mathrm{i}=\mathrm{m}} \Delta f(t_{\mathrm{i}}) \exp\left[\frac{-(t_{\mathrm{m}+1} - t_{\mathrm{i}})}{a} \left(\frac{n\pi}{\ell\ell} \right)^2 \right]$$
$$= (J_{\mathrm{f,n,m}-1} + \Delta f(t_{\mathrm{m}})) \exp\left[\frac{-(t_{\mathrm{m}+1} - t_{\mathrm{m}})}{a} \left(\frac{n\pi}{\ell\ell} \right)^2 \right] \tag{23}$$

$t = t_{\mathrm{m}+1}$) in order to make the solution fully recursive. Not only do we obtain a dramatic reduction in memory and computation requirements, we can also use longer time steps whenever the boundary conditions change negligibly over time. With a thick specimen (>1 in.) and short time steps (0.7 s), the effective Fourier number will possibly be quite small (<0.046). For nine-digit accuracy, this will necessitate the use of the first term of the second series of Eq. (19) for use in Eq. (21) during the non-recursive time interval $t_{\mathrm{m}+1} - 0.05a\ell\ell \le t_{\mathrm{i}} \le t_{\mathrm{m}+1}$ and application of the recursive formulation to the remaining time interval. More practically, with experimental data being no better than three-digit precision, the first eight terms in the first series of Eq. (19) are sufficient (meaning the second series solution is not needed and use of the non-recursive time interval is thereby avoided). This dramatic improvement in computational efficiency should rival some efficient finite difference methods. The intriguing aspect of the discretized solution above is the coupled explicit solutions of heat and moisture transfer, with their order-of-magnitude differences in the time scale of their physical processes. This clearly is an advantage over finite difference methods, which may require specialized matrix equation solvers or additional constructs of elaborate spatial discretizations to overcome the time-scale differences. For the final adjustment, the solution to Eqs (1) and (2), which allows for the temperature and moisture content dependencies of properties, is the same as that for the constant properties, providing we implement the following substitutions [10] prescribed by Eq. (24).

For the Eq. (24) solution, $T(x,t)$ and $Y(x,t)$ are temperature and moisture-potential deviations from initial values for comparing with measured deviation values, whereas $T(x,t)$ and $U(x,t)$ are now considered as transformed variables having the same physical units as temperature and moisture potential.

Calibration with extruded polystyrene foam and measurement for redwood

In calibrating the K-tester we quasi-pulse heated 1-in.-thick aged, extruded-polystyrene foam (a decade-old Dow's blue board) in temperature jumps of 8°C from equilibrium states. We obtained from National Institute of Standards and Technology (NIST) material databank on-line the values and formula for heat capacities and densities of pure polystyrene (SRM-705a) and air as functions of temperature. By using the measured foam's density, the parallel-mass-weighted values for the foam's heat capacity were then calculated to a fairly high degree of accuracy (within three digits precision) and were within measurement errors of Graves *et al.* [4] for similarly aged Dow's blue board. The thermopile substrate is a thermoset laminate (FR4) with a copper cladding (their thicknesses were provided by Lasercomp company), so their nominal thermal properties of heat capacities, thermal conductivity, and density were adopted from Eveloy and others [13]. The total heat absorbed by the foam's volumetric heat capacity after reaching equilibrium (using the third BC solution) was then compared with the total heat transferred

$$T(x,t) = \frac{1}{K_{\mathrm{q}}(Y_0,T_0) + \varepsilon\lambda K_{\mathrm{m}}(Y_0,T_0)\delta} \int_0^{\mathrm{T(x,t)}} (K_{\mathrm{q}}(Y_0,T) + \varepsilon\lambda K_{\mathrm{m}}(Y_0,T)\delta)\mathrm{d}T$$
$$U(x,t) = \frac{1}{K_{\mathrm{m}}(Y_0,T_0)} \int_0^{\mathrm{Y(x,t)}} K_{\mathrm{m}}(Y,T_0)\mathrm{d}Y \tag{24}$$

from the thermopile during pulse heating (using the first BC solution for copper cladding and second BC solution for the FR4). The value for ratio of the micro-temperature changes across the thermopile thickness to the thermopile microvolt signal was adjusted (by using the Excel spreadsheet solver plug-in software), until both the total heat values calculated were in agreement.

The lack of an adequate standard for thermal conductivity of extruded polystyrene foams is because of great variability resulting from manufacturing processes, particularly as they affect foam morphology, concentrations of blowing agents, and internal thermal radiation heat transfers. With known thermal conductivity data for both pure polystyrene [14] and air as functions of temperature, a series-porosity-weighted formula combining these pure state values with a 9% radiative heat conductivity contribution at room temperature was found adequate to fit the data of Graves *et al.* [4] for aged Dow's blue board. This formula was adopted for the current blue board sample. Figure 1 compares temperature predictions with measured values and demonstrates the adequacy of the blue board thermal properties, particularly with correlation coefficients of 0.999 for both upper and lower surfaces. The high noise level of the theoretical solution results from the fairly low values of the thermopile signal related to the quite low heat loading of foam during the 8°C pulse-heating step. The initial lag in temperature rise results from the thermal wave traveling through the structure containing the thermopile even though the heat pulsing began almost immediately. The rise portion of the temperature curve is most sensitive to thermal conductivity of the specimen and heat capacity of the thermopile, whereas the horizontal portion of the temperature curve is most sensitive to heat capacity of the specimen and thermal conductivity of the thermopile.

Figure 2 shows results with the redwood flooring with overall 3% moisture content. To obtain the most uniform property, a long and wide floor board without knots and with cross-grains uniformly along the length was selected. The grooves were planed so that air spaces and use of glue was minimized. After the board sections were glued together, the overall specimen was planed flat to ensure physical contact across the 30 by 30-cm sensing area. Despite this effort there were large variations in density along the board length. Therefore, when our experiments with the K-tester are finished, the center section (10 by 10 cm) of the specimen will be cut out and measured for oven-dried density and moisture content for different RH conditions. At that time we will directly link thermal properties with density, moisture content, and temperature and report it in a table in a later publication. For now we use 'average' values obtained with the board scraps to demonstrate the technique. Because redwood requires a much higher heat load than that of the XPS foam to achieve an 8°C rise, Fig. 2 shows much smoother predictions of upper and lower interface temperatures, with a correlation coefficient of 0.9999. A constant temperature difference of about 0.05°C is maintained between the upper and lower temperatures despite our inputs to the K-tester for both upper and lower temperatures to reach the same 34°C. The derived thermal properties at the mean temperature of 30.2°C are heat capacity of

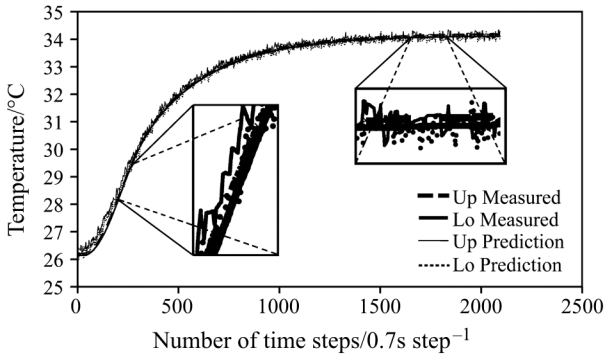

Fig. 1 Surface temperature predictions *vs.* measurements with calibrated thermopile for Dow's aged extruded polystyrene foam

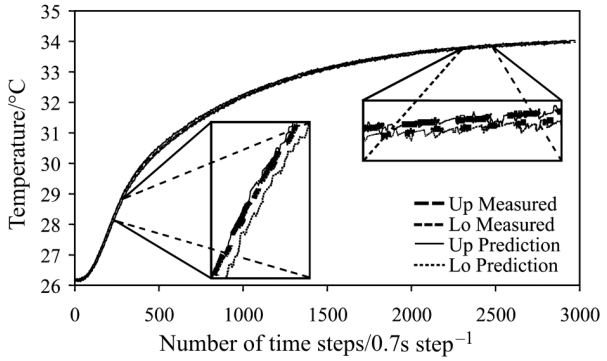

Fig. 2 Center-sensor interface temperature predictions and measurements for redwood flooring specimen (3% moisture content)

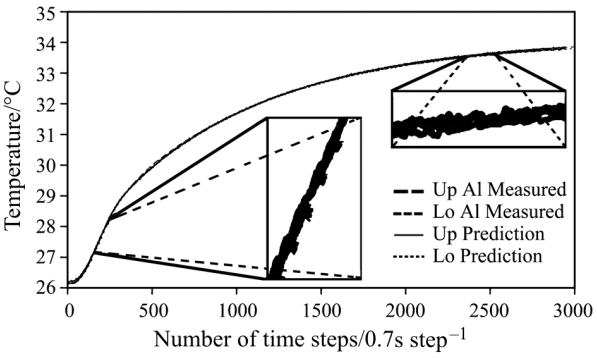

Fig. 3 Center-A1 interface temperature predictions and measurements for redwood flooring specimen (14% moisture content)

1.380 J kg^{-1} K^{-1} and thermal conductivity of 0.0777 W mK^{-1}. If we estimate the oven-dried density as 299 kg m^{-3} and moisture content as 3%, then derived heat capacity and thermal conductivity are respectively 0.6 and 5.3% less than that of the well-known formula [15]. No moisture flow involving the latent heat was needed to achieve the predictive results in Fig. 2.

The redwood specimen was then conditioned in a 90% RH room for at least a couple weeks, and it attained an overall moisture content of 14%. To better seal in moisture during a 24-h test (several 8°C jumps were attempted in a single test run), we used 0.4-mm-thick aluminum 2024-T3 to cover both upper and lower surfaces of the specimen. The thermal properties of 2024-T3 are well known at air temperature from the NIST material databank. Our results with the first BC solution for the aluminum plate show it has a negligible influence on the results because of its high thermal conductivity and low contribution to heat absorbing capacity. The results in Fig. 3 show that highly moist redwood takes longer to reach equilibrium and even a closer fit to the measured values of temperatures, with a correlation coefficient of 0.9999. The derived heat capacity and 'steady' thermal conductivity at the mean temperature of 30.2°C were, respectively, 1.932 J kg^{-1} K^{-1} and 0.0996 W mK^{-1}. Moisture flow with latent heat was needed that provided an equivalent thermal conductivity of 0.0315 W mK^{-1}. This resulted in a total thermal conductivity of 0.1311 W mK^{-1}, or a significant 32% increase over the 'steady' thermal conductivity value. If we once again use the oven-dried density of 299 kg m^{-3} and moisture content of 14%, the derived heat capacity and 'steady' thermal conductivity are, respectively, 10.9 and 4.1% higher than those of the well-known formula [11].

Conclusions

Our efforts to understand heat and moisture transfer in a wood specimen as used in the K-tester has led to an unconventional numerical solution and intriguing protocol to deriving heat and moisture transfer properties. Exact analytical solution to the Luikov's equations for one-dimensional flow in a porous hygroscopic orthotropic material as described in this paper has the following features. The solution was given for three types of stepping boundary conditions: (1) stepping functions of surface temperature and moisture and their surface gradients on just one side of the material, (2) stepping functions of surface temperature and moisture on both sides of the material, and (3) stepping functions of the surface gradients of temperature and moisture on both sides of the material. If short time intervals and reformulation into recursive forms are also used, then the resulting time-discretized solutions are stable, accurate, fast, simple, and cover most practical situations. The recursive solution procedure described in this paper was easily implemented in the Excel spreadsheet with Visual Basic Application (VBA) macros. We demonstrated its use in a spreadsheet to fit the data, and by implication it can be used in a computer code that would be highly competitive with finite difference methods. Indeed it would serve as a benchmark to any finite difference methods used to solve for combined heat and mass transfer, particularly when physical time scales are orders of magnitude different.

The solutions were also used to answer the significance of moisture flow with latent heat as affecting the heat flow within the moist wood. In the case of redwood with about 14% moisture content, the latent heat contribution adds 32% to the steady value of thermal conductivity. With even higher moisture content, particularly near fiber saturation point, perturbation on conductive heat flow will likely be higher, perhaps on the order of 50%.

The quasi-impulse transient method is then a viable concept, particularly for high thermal conductivity materials, because the unidirectional heat flow was verified with four sensors surrounding the central sensor. Indeed, with the new procedure, the current K-tester is no longer limited to low thermal conductivity materials at steady-state conditions. Because the K-tester can range from 10 to 80°C, we plan to examine the moisture and temperature dependencies and compare with known literature values for wood products [2–7, 15]. Because the center sensor data was used in deriving the thermophysical properties, we plan to cut out the 10 by 10-cm center section at the end of the test series to properly assess their material density and moisture contents. Only then can the functional relationship be more accurately ascertained for comparison to known formulations and provided in tables.

The solution method and result also have implications in related fields, such as ignition of moist wood under thermal radiation impulse heating. Because transient moisture mass loss will also occur for this condition (and measured as well), the moisture parameters of mass conductivity and thermogradient coefficient can then be independently determined, rather than adopting the corresponding values for pine wood [6] and adjusting them to fit the data, as was done for this paper.

Acknowledgements

We thank Robert Munson, for upgrading the Lasercomp K-tester 637 and obtaining the data, and Robert White, Ph.D., and Anton TenWolde, Ph.D, for their support of this work.

References

1 G. J. Kluitenberg, J. M. Ham and K. L. Bristow, Soil Sci. Soc. Am. J., 57 (1993) 1444.
2 A. J. Nanassy, Wood Science, 11 (1978) 111.
3 W. Yang, S. Sokhansanj, J. Tang, and P. Winter, Biosystems Engineering 82, Pt. 2 (2002) 169.
4 R. S. Graves, D. W. Yarbrough, D. L. McElroy, and H. A. Fine, Insulation Materials: Testing and Applications, 2nd Volume, ASTM STP 1116, Graves and Wysocki, (Eds.), American Society for Testing and Materials, Philadelphia, 1991.
5 W.J. Parker, Prediction of the Heat Release Rate of Wood, Ph.D. Dissertation, School of Engineering & Applied Science, George Washington University, Washington, D. C., 1988.
6 A.V. Luikov, Heat and Mass Transfer in Capillary-Porous Bodies, Pergamon Press, Oxford, 1966, Chapter 7.
7 J. Y. Liu, Journal of Heat Transfer, 113 (1991) 757.
8 R.C. Gaur and N.K. Bansal, Int. J. of Energy Res., 23 (1999) 875.
9 D. Song, Z. S. Liu, and G. Wang, Numerical Heat Transfer, Part A, 42 (2002) 585.
10 H. S. Carslaw and J. C. Jaeger, Conduction of Heat in Solids, 2nd edition reprint, Oxford University Press, 1960, Chapters 1 and 3.
11 L. Zhou, V. M. Puri and R. C. Anantheswaran, Drying Technology, 12 (1994) 607.
12 A. L. Rabenstein, Elementary Differential Equations with Linear Algebra, Academic Press, New York and London, 1971.
13 V. Eveloy, P. Rodgers, and J. Lohan, Proc. 3rd Int. Conf. on Thermal and Mechanical Simulation in Microelectronics, Paris, France, April 14–16 2002.
14 Y. Agari, M. Shimada, and A. Ueda, Polymer, 38 (1997) 2649.
15 T. Wolde, J.D. McNatt and L. Krahn, Thermal Properties of Wood and Wood Panel Products for Use in Buildings, DOE/USDA-21697/1 and ORNL/Sub/87-21697/1, 1988.

DOI: 10.1007/s10973-005-7068-y